Geomechanics and Engineering, *Vol. 31, No. 4 (2022) 375-384*
https://doi.org/10.12989/gae.2022.31.4.375

Three-dimensional stability assessment of slopes with spatially varying undrained shear strength

Yunwei Shi[a], Xianqi Luo* and Pingfan Wang[b]

School of Naval Architecture, Ocean & Civil Engineering, Shanghai Jiao Tong University, 800 Dongchuan Road, Minhang District, Shanghai, China

(*Received March 12, 2022, Revised November 8, 2022, Accepted November 14, 2022*)

Abstract. The variation of the undrained shear strength (c_u) is an important consideration for assessing slope stability in engineering practice. Previous studies focused on the three-dimensional (3D) stability of slopes in normally consolidated clays generally assume the undrained shear strength increases linearly with depth but does not vary in the horizontal direction. To assess the 3D stability of slopes with spatially varying undrained shear strength, the kinematic approach of limit analysis was adopted to obtain the upper bound solution to the stability number based on a modified failure mechanism. Three types failure mechanism: the toe failure, face failure and below-toe failure were considered. A serious of charts was then presented to illustrate the effect of key parameters on the slope stability and failure geometry. It was found that the stability and failure geometry of slopes are significantly influenced by the gradient of c_u in the depth direction. The influence of c_u profile inclination on the slope stability was found to be pronounced when the increasing gradient of c_u in the depth direction is large. Slopes with larger width-to-height ratio B/H are more sensitive to the variation of c_u profile inclination.

Keywords: 3D slope stability; failure mechanism; limit analysis; spatially varying strength

1. Introduction

The undrained stability analysis of slopes and excavations has long been of interest to the community of geotechnical engineering. When assessing the undrained stability of slopes or excavations in normally consolidated clays, the undrained shear strength c_u was generally assumed to linearly increase with depth (Gibson and Morgenstern 1965, Hunter and Schuster 1968, Kumar *et al.* 2014). Koppula (1984) assessed the stability of slopes with linearly increasing c_u, where the undrained strength is positive finite on the top surface of the slope. The results demonstrated the variation ratio of c_u significantly affects the slope stability and the depth of failure surface. Griffiths and Yu (2015) investigated the influence of a firm stratum on the stability and failure surface of slopes with linearly increasing c_u. The zero strength at the crest level was also examined. Li *et al.* (2018) developed a closed-form solution to evaluate the stability of slopes in clay with linearly increasing c_u in the framework of limit equilibrium method. The difference in the safety factor between a slope with tension crack and a slope without a crack becomes more significant with an increase in the variation ratio of c_u. Three-dimensional analyzes were also carried out (Zhou *et al*. 2019, Ukritchon *et al*. 2020), however, the effect of linearly increase c_u on the 3D failure geometry of slopes were only investigated under specific conditions (Li *et al.* 2009, 2010).

In engineering practice, it is found that the c_u of clays or other geomaterials may also vary in the lateral direction as a result of geologic history, lithology, depositional conditions and chemistry process (Bjerrum 1967, Skempton *et al.* 1969, Rahardjo *et al.* 1995, Mesri and Shahien 2003). Recently, Hossley and Leshchinsky (2019) adopted the lower bound finite-element limit analysis to study the influence of spatially varying c_u on the stability and failure geometry of slopes. The results indicated the changing c_u profile significantly affects the slope stability by changing the observed failure geometry. Ke *et al.* (2021) conducted parametric studies to assess the influence of the strength variation in the horizontal direction on bearing capacity of strip footing near slopes. Nevertheless, aforementioned studies are limited to 2D condition, a 3D analysis is favored when the dimension of a slope is limited by existing structures or designing excavations where the geometry is well defined.

Historically, the stability of slopes has been assessed using various numerical methods, such as finite element method (Azhari and Ozbay 2018, Naeij *et al.* 2021, Satyanaga *et al.* 2022), discrete element method (Bonilla-Sierra *et al.* 2015, Weng *et al.* 2019, Gao *et al.* 2020, 2021), material point method (Bhandari *et al.* 2016, Feng and Xu 2021) and smooth particle hydrodynamics (Bui *et al.* 2011, Ray *et al.* 2019). Numerical methods have advantages in dealing with slopes with complicated geometric forms and loading conditions (Zhang *et al.* 2013, Tran *et al.* 2019, Zhang *et al.* 2019, Hassanikhah and Drumm 2020),

*Corresponding author, Ph.D.
E-mail: luoxianqi402@yeah.net
[a]Ph.D. Student
E-mail: yunwei_shi@yeah.net
[b]Ph.D. Student
E-mail: pingfan.wang@sjtu.edu.cn

ISSN: 2005-307X (Print), 2092-6219 (Online)

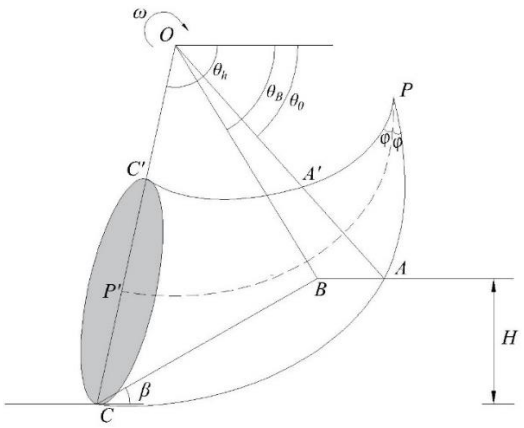

Fig. 1 Failure mechanism proposed by Michalowski and Drescher (2009)

therefore they are extensively adopted for case studies (Bi *et al*. 2019, Azarafza *et al.* 2021). The limitation of numerical methods lies in the intensive computational effort when carrying out parametric studies. In contrast, the analytical approaches including the limit-equilibrium method (Deng *et al.* 2019, Farshidfar *et al.* 2021) and the limit analysis method (Luo *et al*. 2021, Rao *et al.* 2021, Chehade *et al.* 2022) are more convenient for performing parametric studies. The limit-equilibrium method is the most common method used in engineering practice. Despite its popularity, some limitations still exist in the assumptions with respect to the inter-column forces, the direction of resultant shear resistance and moment equilibrium conditions (Zhou and Qin 2020). The limit analysis method offers a rigorous upper/lower bound for slope stability problems by constructing the kinematically admissible velocity field/statically admissible stress field (Chen 1975). A notable merit of the kinematic approach of limit analysis lies in no stress field involved in the calculation process, a rigorous upper bound solution to the critical slope height or the factor of safety can be obtained by assuming a reasonable slip surface. The results obtained by the kinematic approach of limit analysis have been proved to be credible (Chen 1975, Zhang *et al.* 2016).

In this paper, the 3D stability of slopes with spatially varying undrained shear strength was investigated using the kinematic approach of limit analysis. The upper bound solution to the stability number was derived. The failure mechanisms including the below-toe failure, toe failure and face failure were accounted for to capture the most critical condition. Then a serious of charts was presented to discuss the effect of key parameters on the slope stability and failure geometry.

2. Kinematic approach of limit analysis

The kinematic approach of limit analysis, also known as the upper bound limit analysis method requires that the rate of dissipation within the plastic zone be equated to the rate of external work of the failing mass. The application of limit analysis in geotechnical engineering was formulated systematically by Chen (1975).

In the framework of kinematic approach of limit analysis, Chen (1975) adopted the log-spiral rotational failure surface to assess 2D slope stability. With respect to the 3D analysis, Michalowski and Drescher (2009) proposed a horn-like failure mechanism which has been the most commonly used mechanism during the last decade (He *et al.* 2015, Gao *et al.* 2016, Yang and Xu, 2017, Wang *et al.* 2019). As shown in Fig. 1, the underlying requirement was the center line *PP*' cannot intersect the slope. Park and Michalowski (2018) further modified the failure mechanism to lift the restriction, so that the center line of the curvilinear cone can intersect the slope. And this modified failure mechanism was adopted in the study to capture the most critical condition. Note that when dealing with soils with varied friction angle, the failure mechanism is no longer valid.

3. Assumptions

To facilitate the 3D stability analysis of slopes with spatially varying undrained shear strength, following assumptions are made:

1) linear Mohr-Coloumb failure criterion is satisfied.

2) soils are ideal rigid and perfectly plastic with an associated normality rule.

4. Methodologies

4.1 Undrained shear strength profile

The undrained shear strength profile considered in this study in depicted in Fig. 2. In the figure, the slope with height H and angle β is made of soil with a unit weight γ. For the ease of the measurement of soil strength before excavation work, the origin point is set at the slope crest. The soil exhibits a linear increase in undrained shear strength with depth but also varies in the lateral direction.

The undrained shear strength can be defined using the c_u profile inclination α, where counterclockwise is positive. Then the undrained strength at any point can be defined as (Ke *et al*. 2021)

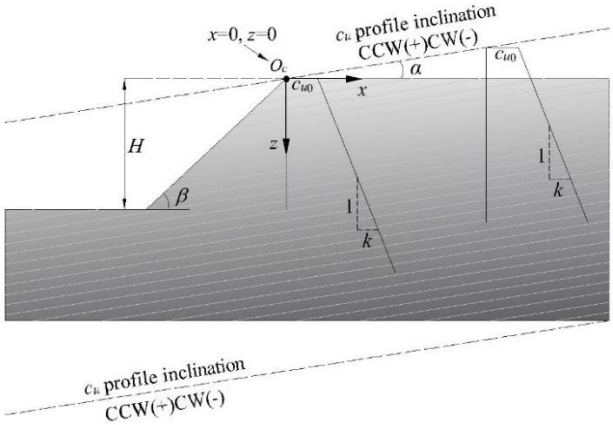

Fig. 2 Problem depiction and notation

$$c_u(x,z) = c_{u0} + k(z + x\tan\alpha) \tag{1}$$

where x is the horizontal location of a given point, z is the depth of a given point measured form the slope top surface, k is the strength gradient in the depth direction, c_{u0} is the initial undrained shear strength at the slope crest (x=0, z=0).

In order to facilitate the parametric study, a dimensionless strength gradient parameter introduced by Hunter and Schuster (1968) is adopted

$$M = \frac{c_{u0}}{kH} \tag{2}$$

4.2 Failure Mechanism

For the undrained analysis, the failure mechanism becomes a torus, as shown in Fig. 3. Three types failure mechanism: the toe failure, face failure and below-toe failure are considered. Note that when $\beta'=\beta$ (Fig. 3(a)), the below-toe failure becomes the toe failure. And the face failure is a special case of toe failure with a smaller slope height H' (Fig. 3(b)). The following equations are formulated based on the below-toe failure mechanism.

The trace of the failure mechanism on the symmetry plane is described by two circular arc AD and AD', which can be respectively expressed as

$$r = r_0 \tag{3}$$

$$r' = r_0' \tag{4}$$

The mechanism is generated by rotating a circle defined by the arc given in Eqs. (3) and (4) around the axis passing through the rotation center O. The distance from the rotation center O to the axis of the torus r_m and the radius of the circle R can be expressed as

$$r_m = \frac{r_0 + r_0'}{2} \tag{5}$$

$$R = \frac{r_0 - r_0'}{2} \tag{6}$$

In the polar coordinate system, the contour of the slope can be described as a piece - wise function

$$r_s(\theta) = \begin{cases} \dfrac{r_0\sin\theta_0}{\sin\theta}, & \theta_0 < \theta \le \theta_B \\ \dfrac{r_0\sin(\beta+\theta_h)}{\sin(\beta+\theta)}, & \theta_B < \theta \le \theta_C \\ \dfrac{r_0\sin\theta_h}{\sin\theta}, & \theta_C < \theta \le \theta_h \end{cases} \tag{7}$$

Also the x and z coordinate for the c_u profile can be expressed as

$$x = r_0(\cos\theta - \cos\theta_h) - H\cot\beta' \tag{8}$$

$$z = r_0(\sin\theta - \sin\theta_0) \tag{9}$$

Fig. 4 shows the mechanism for the slope with finite width B modified with a block of width b. When b approaches infinity, the 3D failure mechanism is transformed to the 2D failure mechanism.

4.3 Objective function

Based on the failure mechanism shown in Fig. 3(a), the safety factor or the stability number can be derived.

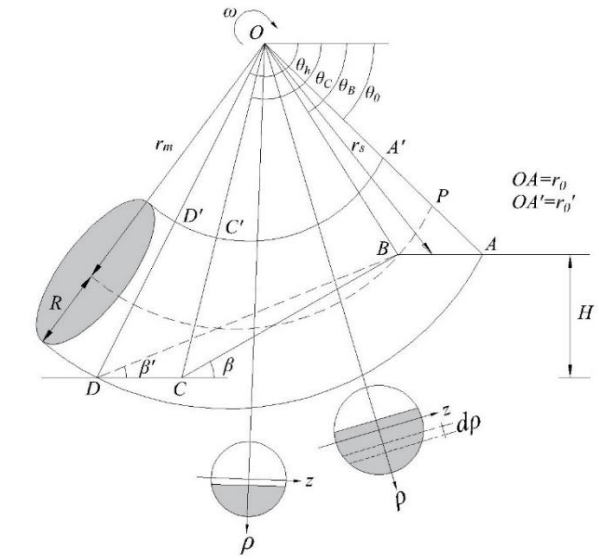

(a) Below-toe failure

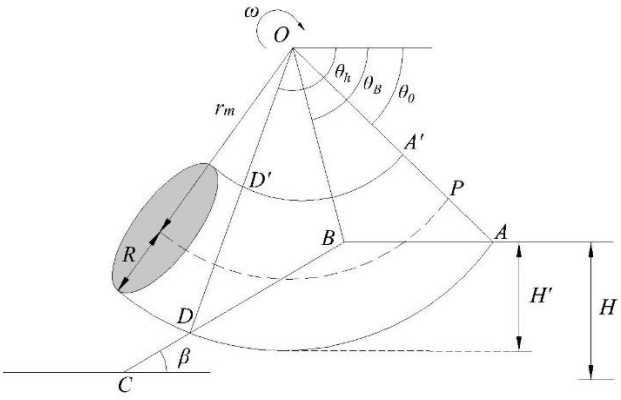

(b) Face failure

Fig. 3 Three-dimensional undrained failure mechanism

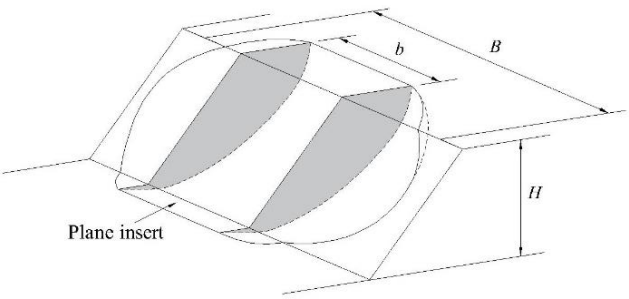

Fig. 4 Mechanism with plane insert

The external work rate of soil weight for the torus can be expressed as

$$W_{\gamma}^{3D} = 2\omega\gamma\int_{\theta_0}^{\theta_h}\int_{r_s}^{r}\rho^2\cos\theta\sqrt{R^2-\left(\rho-r_m\right)^2}\,d\rho d\theta \quad (10)$$

The external work rate of soil weight for the plane insert can be expressed as

$$W_{\gamma}^{2D} = \gamma\omega r_0^3\left(f_1 - f_2 - f_3 - f_4\right) \quad (11)$$

where f_1-f_4 can be expressed as

$$f_1 = \frac{\sin\theta_h - \sin\theta_0}{3} \quad (12)$$

$$f_2 = \frac{1}{6}\sin\theta_0\frac{L}{r_0}\left(2\cos\theta_0 - \frac{L}{r_0}\right) \quad (13)$$

$$f_3 = \frac{1}{6}\left[\sin\left(\theta_h-\theta_0\right) - \frac{L}{r_0}\sin\theta_h\right]\left(\cos\theta_h + \cos\theta_0 - \frac{L}{r_0}\right) \quad (14)$$

$$f_4 = \left(\frac{H}{r_0}\right)^2\frac{\cot\beta' - \cot\beta}{2}\left[\cos\theta_0 - \frac{L}{r_0} - \frac{H}{r_0}\frac{\cot\beta+\cot\beta'}{3}\right] \quad (15)$$

where H/r_0 and L/r_0 can be expressed as

$$\frac{H}{r_0} = \sin\theta_h - \sin\theta_0 \quad (16)$$

$$\frac{L}{r_0} = \frac{\sin\left(\theta_h-\theta_0\right)}{\sin\theta_h} - \frac{\sin\left(\theta_h+\beta'\right)}{\sin\theta_h\sin\beta'}\left(\sin\theta_h - \sin\theta_0\right) \quad (17)$$

Then the total external work rate can be expressed as

$$W_{\gamma} = W_{\gamma}^{3D} + b\cdot W_{\gamma}^{2D} \quad (18)$$

Due to the rigid body assumption, the internal energy dissipation inside the sliding body is ignored. The internal energy dissipation rate along the failure surface of the torus can be expressed as

$$D^{3D} = 2c_u\left(x,z\right)\omega\int_{\theta_0}^{\theta_h}\int_{r_s}^{r}\rho^2\frac{R}{\sqrt{R^2-\left(\rho-r_m\right)^2}}\,d\rho d\theta \quad (19)$$

The internal energy dissipation rate of the plane insert can be expressed as

$$D^{2D} = \int_{\theta_0}^{\theta_h} c_u\left(x,z\right)vr_0 d\theta = \omega r_0^2\int_{\theta_0}^{\theta_h} c_u\left(x,z\right)d\theta \quad (20)$$

Then the total internal energy dissipation rate can be expressed as

$$D_{\text{int}} = D^{3D} + b\cdot D^{2D} \quad (21)$$

Based on the gravity increase method, the safety factor can be defined as (Yang and Li 2018)

$$F_s = \frac{D_{\text{int}}}{W_{\gamma}} \quad (22)$$

Then a dimensionless stability number N_s can be obtained

$$N_s = F_s\cdot\frac{\gamma}{k} \quad (23)$$

To yield the least upper bound solution to N_s, an optimization procedure with respect to the unknown parameters (θ_0, θ_h, r'/r and β') was coded in MATLAB. The optimization procedure proposed by Chen (1992) was adopted herein. An initial estimate of the unknown parameters can be obtained by the random search method, then the global minimum can be searched by the optimization procedure.

Table 1 Comparison with Park and Michalowski (2018)

		$\gamma H/c_{u0}$	
β	B/H	This study	Park and Michalowski (2018)
30º	0.5	16.644	16.645
30º	1	10.792[a]	10.797[a]
30º	3	7.398[a]	7.389[a]
45º	0.5	12.812	12.789
45º	1	9.020[a]	9.021[a]
45º	3	6.795[a]	6.783[a]
60º	0.5	10.865	10.860
60º	1	7.821	7.821
60º	3	6.022	6.022

[a]: Below-toe failure

5. Comparison

To validate the formulation and the optimization procedure. The solution in the study is degenerated into the homogeneous condition. Herein the calculated dimensionless critical slope height $\gamma H/c_{u0}$ are compared with those obtained by Park and Michalowski (2018), as shown in Table 1. It is clear that the present solutions agree well with the result of Park and Michalowski (2018).

The special case of linearly increasing undrained shear strength with c_u=0 (M=0) at the slope crest level under 2D condition was examined by Griffiths and Yu (2015). The present solution will become 2D cases when B/H approaches infinity, the stability number N_s obtained using the proposed approach are 8.511, 4.106 and 2.563 for β=15º, 45º and 75º respectively. These results are identical with those obtained by Griffiths and Yu (2015) as indicated in Fig. 7 in their original work. Then the validity of the proposed approach and optimization procedure is confirmed.

6. Results and discussions

To capture the influence of key parameters on the slope

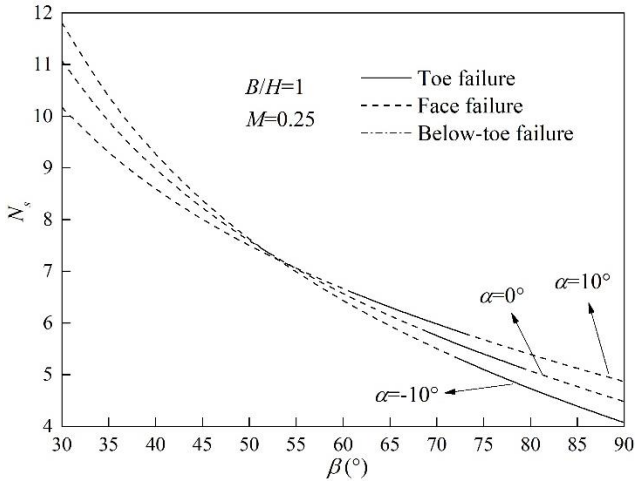

(a) M=0.25

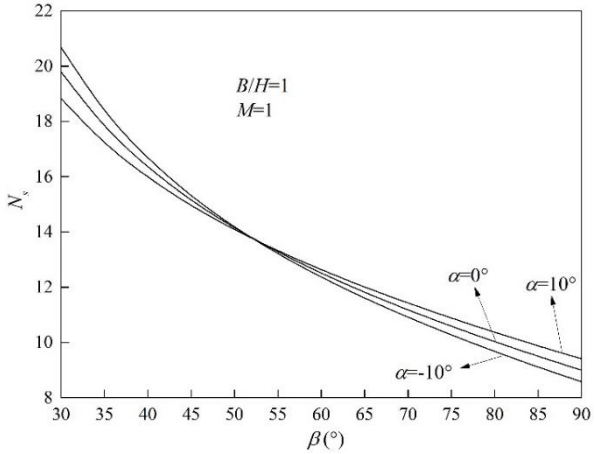

(b) M=1

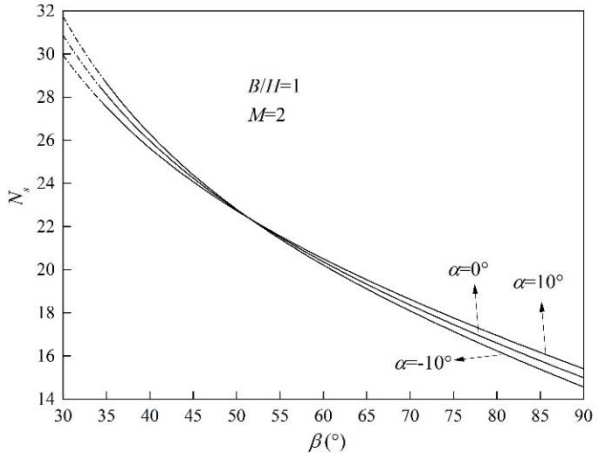

(c) M=2

Fig. 5 Stability number against slope angle

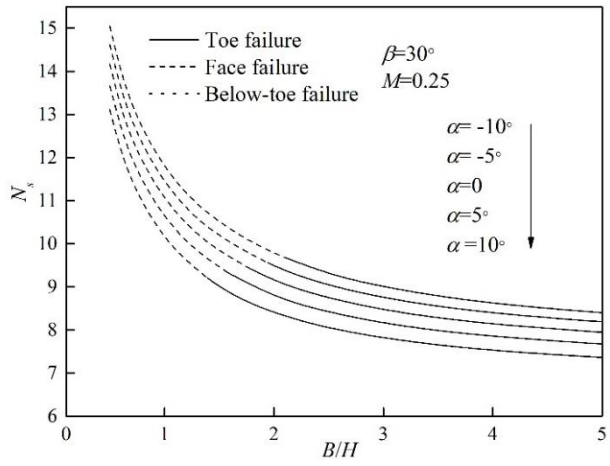

(a) M=0.25

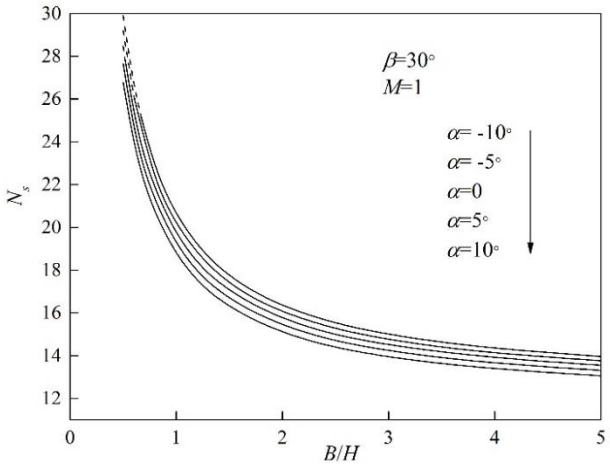

(b) M=1

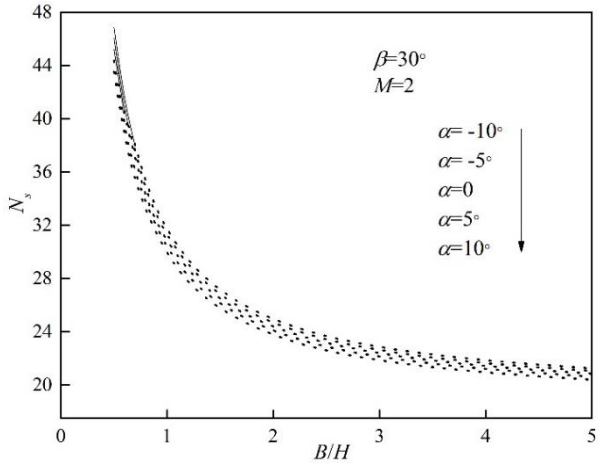

(c) M=2

Fig. 6 Stability number against B/H with β=30º

stability and failure geometry, a series of charts will be developed in the following.

Fig. 5 illustrates the variation of the stability number N_s with slope angle β for different values of c_u profile inclination α. Manifestly, with the increase of α, N_s increases for steep slopes, while a decrease is observed in gentle slopes. Herein the slope angle varies from 30º to 90º, when β locates at both ends, the effect of α on the slope stability is pronounced, while the influence of α becomes insignificant when β gets the intermediate value. This is because the origin point in the c_u profile is located at the slope crest. When β gets the intermediate value between 30º and 90º, the effect of weakened strength and the enhanced strength on both sides of the z-axis tend to cancel each other out. Moreover, the increase of M gives rise to N_s. With the increase of M, the effect of α on N_s decreases. For example,

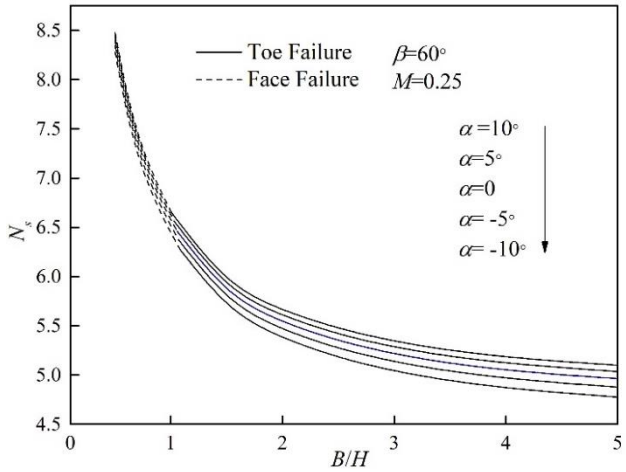

(a) M=0.25

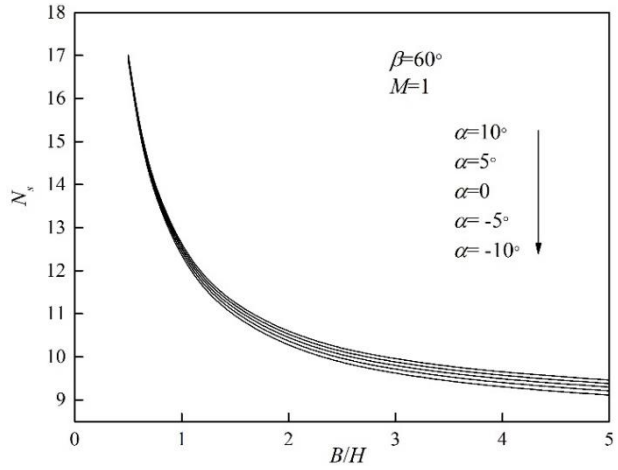

(b) M=1

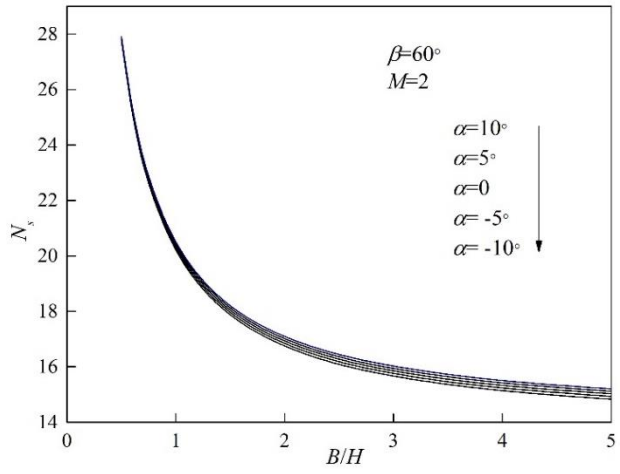

(c) M=2

Fig. 7 Stability number against B/H with β=60º

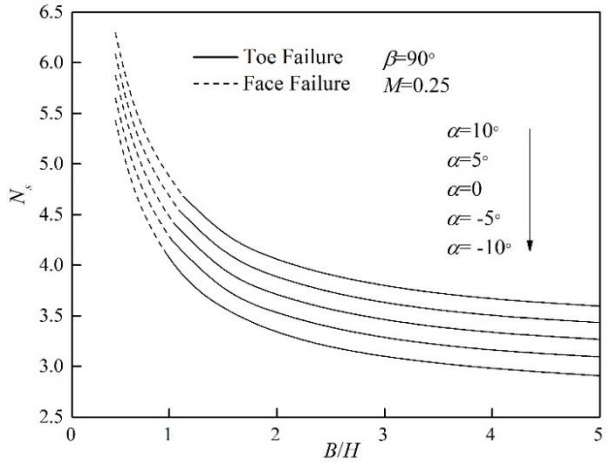

(a) M=0.25

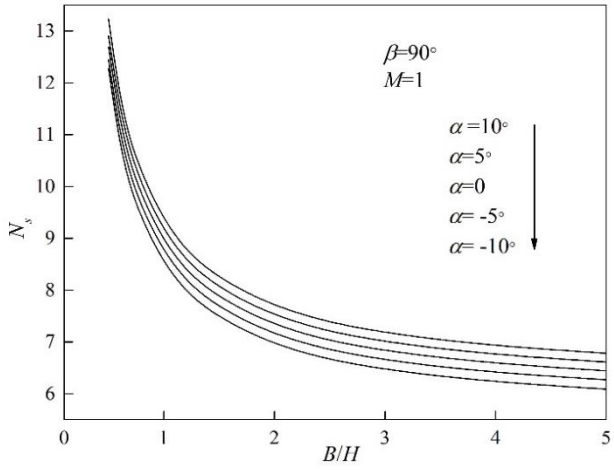

(b) M=1

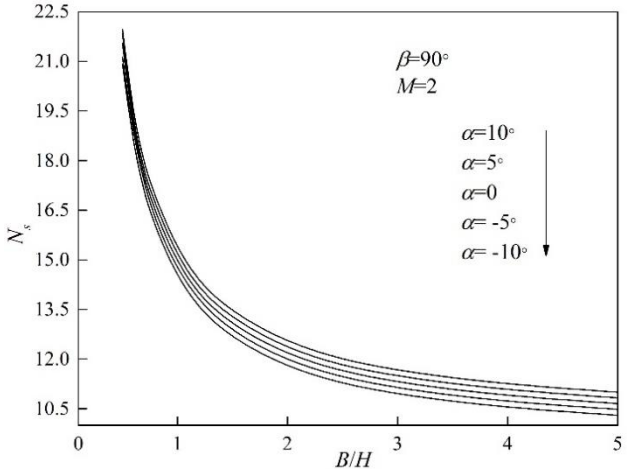

(c) M=2

Fig. 8 Stability number against B/H with β=90º

when the slope angle is 90º, for α varying from -10º to 10º, an increase of 19.5%, 9.7% and 5.8% can be observed respectively for M=0.25, 1, and 2.

From Fig. 5, it can also be found that the failure geometry is significantly affected by M. The face failure is produced when M=0.25, and the below-toe failure is observed for M=2. When M is small, the face failure can be observed in both gentle and steep slopes. This is because the dimensionless number M denotes the reciprocal of the increasing rate of c_u in the depth direction. Then a smaller M represents a larger increase in c_u in the depth direction, the large difference in the strength between the upper and lower layer makes the failure occurs in the upper layer. With the increase of M, the soil becomes more uniform, then the failure trends will be similar to those observed in homogeneous slope (Park and Michalowski 2018). And as

shown in Fig. 5(c), for a large M value, the below-toe failure is produced in gentle slopes.

The variation of N_s with B/H for different β and α is shown in Figs. 6-8. With the increase of B/H from 0.5 to 5, N_s decreases sharply at early stage, and then the decreasing trend is reduced. And it is expected that with the further increase of B/H, the solution will approach the 2D solution, then a 2D analysis will significantly underestimate N_s when the slope is constrained in a narrow width. Moreover, it is found that steep slopes with larger B/H are more sensitive to the variation of α than those with small B/H. For instance, for a 90º slope with M=0.25, when α varies from -10º to 10º, an increase of 24% in N_s can be observed when B/H=5, while for B/H=0.5, this value reduces to 16%.

For gentle slopes (30º in this case), the most critical failure mechanism was found to be toe failure when B/H is small in homogenous soil (Park and Michalowski 2018). While in current research, it can be seen from Fig. 6(c) that with a large M value, the toe failure can only be observed when α is small. For α=5º and 10º, the below-toe failure yields the least upper bound solution for all B/H considered. This is because with the increase of α, the strength of the foundation soil is weakened, then the failure surface tends to get deeper and pass below the slope toe. The failure mechanism passing below the slope toe would generate less internal rates of work than the toe failure mechanism, which yields a lower stability number. Additionally, it can also be observed that the face failure occurs only when B/H is small for M=0.25. This reveals the significant influence of the end boundary effect, a toe failure mechanism cannot be constructed with limited slope width.

7. Conclusions

Based on the kinematic approach of limit analysis, this study conducted an analysis on the 3D stability of slopes with spatially varying undrained shear strength. A modified failure mechanism was adopted to derive the least upper bound solution to the stability number. The effects of spatially varying undrained shear strength parameters and the width-to-height ratio on the stability and failure geometry of slopes were investigated. The main findings cane be summarized as follows:

• With the increase of c_u profile inclination α, the stability number N_s increases for steep slopes, while a decrease is observed in gentle slopes. With the increase of the dimensionless factor M, the slope stability becomes less sensitive to the variation of α. Slopes with larger width-to-height B/H are more sensitive to the variation of α. Larger increase of N_s with M is found in steeper slopes.

• The failure geometry is significantly affected by M. The face failure can only be observed when M is small and the below-toe failure is produced when M is large. For a large value of M, the influence of α on the slope stability is not significant, but its influence on the failure geometry in gentle slopes is pronounced.

• This research adopted a semi-analytical method to evaluate the 3D slope stability. Further work should focus on the development of efficient numerical methods for more complex 3D problems, to model the progressive failure process, the influence of seismic forces and complex loading conditions properly.

Acknowledgments

The research described in this paper was financially supported by the National Natural Science Foundation of China (Project No.: 51208301). The authors wish to express their gratitude for the above financial support.

References

Azarafza, M., Bonab, M.H. and Akgun, H. (2021), "Numerical analysis and stability assessment of complex secondary toppling failures: A case study for the south pars special zone", *Geomech. Eng.*, **27**(5), 481-495. https://doi.org/10.12989/gae.2021.27.5.481.

Azhari, A. and Ozbay, U. (2018), "Role of geometry and stiffness contrast on stability of open pit mines struck by earthquakes", *Geotech. Geol. Eng.*, **36**(2), 1249-1266. https://doi.org/10.1007/s10706-017-0390-x.

Bhandari, T., Hamad, F., Moormann, C., Sharmai, K.G. and Westrich, B. (2016), "Numerical modelling of seismic slope failure using MPM", *Comput. Geotech.*, **75**, 126-134. https://doi.org/10.1016/j.compgeo.2016.01.017.

Bi, J.F., Luo, X.Q., Zhang, H.T. and Shen, H. (2019), "Stability analysis of complex rock slopes reinforced with prestressed anchor cables and anti-shear cavities", *Bull. Eng. Geol. Environ.*, **78**(2), 2027-2039. https://doi.org/10.1007/s10064-017-1171-8.

Bjerrum, L. (1967), "Engineering geology of Norwegian normally consolidated marine clays as related to settlements of buildings", *Geotechnique*, **17**(2), 83-118. https://doi.org/10.1680/geot.1967.17.2.83.

Bonilla-Sierra, V., Scholtes, L., Donze, F.V. and Elmouttie, M.K. (2015), "Rock slope stability analysis using photogrammetric data and DFN–DEM modelling", *Acta Geotech.*, **10**(4), 497-511. https://doi.org/10.1007/s11440-015-0374-z.

Bui, H.H., Fukagawa, R., Sako, K. and Wells, J.C. (2011), "Slope stability analysis and discontinuous slope failure simulation by elasto-plastic smoothed particle hydrodynamics (SPH)", *Geotechnique*, **61**(7), 565-574. https://doi.org/10.1680/geot.9.P.046.

Chehade, H.A., Dias, D., Sadek, M., Jenck, O. and Chehade, F.H. (2022), "Seismic internal stability of saturated reinforced soil retaining walls using the upper bound theorem of limit analysis", *Soil Dyn. Earthq. Eng.*, **155**, 107180. https://doi.org/10.1016/j.soildyn.2022.107180.

Chen, W.F. (1975), *Limit Analysis and Soil Plasticity*, Elsevier Scientific Publishing Company, New York, NY, USA.

Chen, Z.Y. (1992), "Random trials used in determining global minimum factors of safety of slopes", *Can. Geotech. J.*, **29**(2), 225-233. https://doi. org/ 10. 1139/ t92- 026.

Deng, D.P., Lu, K. and Li, L. (2019), "LE analysis on unsaturated slope stability with introduction of nonlinearity of soil strength", *Geomech. Eng.*, **19**(2), 179-191. https://doi.org/10.12989/gae.2019.19.2.179.

Farshidfar, N., Keshavarz, A. and Mirhosseini, S.M. (2021), "Seismic stability of reinforced soil slopes using the modified pseudo-dynamic method", *Earthq. Struct.*, **20**(5), 473-486. https://doi.org/10.12989/eas.2021.20.5.473.

Feng, Z.K. and Xu, W.J. (2021), "GPU material point method (MPM) and its application on slope stability analysis", *Bull. Eng. Geol. Environ.*, **80**(7), 5437-5449. https://doi.org/10.1007/s10064-021-02265-8.

Gao, G., Meguid, M.A., Chouinard, L.E. and Xu, C. (2020), "Insights into the transport and fragmentation characteristics of earthquake-induced rock avalanche: Numerical study", *Int. J. Geomech.*, **20**(9), 04020157. https://doi.org/10.1061/(ASCE)GM.1943-5622.0001800.

Gao, G., Meguid, M.A., Chouinard, L.E. and Zhan, W.W. (2021), "Dynamic disintegration processes accompanying transport of an earthquake-induced landslide", *Landslides.*, **18**(3), 909-933. https://doi.org/10.1007/s10346-020-01508-1.

Gao, Y.F., Wu, D., Zhang, F., Lei, G.H., Qin, H.Y. and Qiu, Y. (2016), "Limit analysis of 3D rock slope stability with non-linear failure criterion", *Geomech. Eng.*, **10**(1), 59-76. https://doi.org/10.12989/gae.2016.10.1.059.

Gibson, R.E. and Morgenstern, N. (1962), "A note on the stability of cuttings in normally consolidated clays", *Geotechnique*, **12**(3), 212-216. https://doi.org/10.1680/geot.1962.12.3.212.

Griffiths, D.V. and Yu, X. (2015), "Another look at the stability of slopes with linearly increasing undrained strength", *Geotechnique*, **65**(10), 824-830. https://doi.org/10.1680/jgeot.14.T.030.

Hassanikhah, A. and Drumm, E.C. (2020), "Stability and evolution of planar and concave slopes under unsaturated and rainfall conditions", *Int. J. Geomech.*, **20**(7), 04020099. https://doi.org/10.1061/(ASCE)GM.1943-5622.0001662.

He, Y., Hazarika, H., Yasufuku, N., Han, Z. and Li, Y.G. (2015), "Three-dimensional limit analysis of seismic displacement of slope reinforced with piles", *Soil Dyn. Earthq. Eng.*, **77**, 446-452. http://dx.doi.org/10.1016/j.soildyn.2015.06.015.

Hossley, A. and Lenshchinsky, B. (2019), "Stability and failure geometry of slopes with spatially varying undrained shear strength", *J. Geotech. Geoenviron. Eng.*, **145**(5), 06019002. https://doi.org/10.1061/(ASCE)GT.1943-5606.0002046.

Hunter, J.H. and Schuster, R.L. (1968), "Stability of simple cuttings in normally consolidated clays", *Geotechnique*, **18**(3), 372-378. https://doi.org/10.1680/geot.1968.18.3.372.

Ke, L.J., Gao, Y.F., Zhao, Z.H., Zhou, Y.D. and Ji, J. (2021), "Undrained bearing capacity of strip footing near slopes considering the orientation of strength increase", *Int. J. Geomech.*, **21**(7), 06021016. https://doi.org/10.1061/(ASCE)GM.1943-5622.0002088.

Koppula, S.D. (1984), "On stability of slopes in clays with linearly increasing strength", *Can. Geotech. J.*, **21**(3), 577-581. https://doi.org/10.1139/t84-059.

Kumar, J., Chakraborty, M. and Sahoo, J.P. (2014), "Stability of unsupported vertical circular excavations", *J. Geotech. Geoenviron. Eng.*, **140**(7), 04014028. https://doi.org/10.1061/(ASCE)GT.1943-5606.0001118.

Li, A.J., Merifield, R.S. and Lyamin, A.V. (2009), "Limit analysis solutions for three dimensional undrained slopes", *Comput. Geotech.*, **36**(8), 1330-1351. https://doi.org/10.1016/j.compgeo.2009.06.002.

Li, A.J., Merifield, R.S. and Lyamin, A.V. (2010), "Three-dimensional stability charts for slopes based on limit analysis methods", *Can. Geotech. J.*, **47**(12), 1316-1334. https://doi.org/10.1139/T10-030.

Li, B., Zhang, F. and Wang, D. (2018), "Impact of crack on stability of slope with linearly increasing undrained strength", *Math. Probl. Eng.*, **2018**, 1096513. https://doi.org/10.1155/2018/1096513.

Li, W., Li, J.B., Tang, G.P., Chen, J.Y. and Dai, C.L. (2021), "Upper-bound limit analysis for slope stability based on modified Mohr-Coulomb failure criterion with tensile cutoff", *Int. J. Geomech.*, **21**(10), 04021184. https://doi.org/10.1061/(ASCE)GM.1943-5622.0002154.

Mesri, G. and Shahien, M. (2003), "Residual shear strength mobilized in first-time slope failures", *J. Geotech. Geoenviron. Eng.*, **129**(1), 12-31. https://doi.org/10.1061/(ASCE)1090-0241(2003)129:1(12).

Michalowski, R.L. and Drescher, A. (2009), "Three-dimensional stability of slopes and excavations", *Geotechnique*, **59**(10), 839-850. https://doi.org/10.1680/geot.8.P.136.

Naeij, M., Ghasemi, H., Ghafarian, D. and Javanmardi, Y. (2021), "Explicit finite element analysis of slope stability by strength reduction", *Geomech. Eng.*, **26**(2), 133-146. https://doi.org/10.12989/gae.2021.26.2.133.

Nian, T.K., Jiang, J.C., Wang, F.W., Yang, Q. and Luan, M.T. (2016), "Seismic stability analysis of slope reinforced with a row of piles", *Soil Dyn. Earthq. Eng.*, **84**, 83-93. https://doi.org/10.1016/j.soildyn.2016.01.023.

Park, D. and Michalowski, R.L. (2018), "Intricacies in three-dimensional limit analysis of earth slopes", *Int. J. Numer. Anal. Methods Geomech.*, **42**(17), 2109-2129. https://doi.org/10.1002/nag.2846.

Rahardjo, H., Lim, T.T., Chang, M.F. and Fredlund, D.G. (1995), "Shear-strength characteristics of a residual soil", *Can. Geotech. J.*, **32**(1), 60-77. https://doi.org/10.1139/t95-005.

Rao, P.P., Wu, J., Jiang, G.Y., Shi, Y.W., Chen, Q.S. and Nimbalkar, S. (2021), "Seismic stability analysis for a two-stage slope", *Geomech. Eng.*, **27**(2), 189-196. https://doi.org/10.12989/gae.2021.27.2.189.

Ray, R., Deb, K. and Shaw, A. (2019), "Pseudo-Spring smoothed particle hydrodynamics (SPH) based computational model for slope failure", *Eng. Anal. Bound. Elem.*, **101**, 139-148. https://doi.org/10.1016/j.enganabound.2019.01.005.

Satyanaga, A., Moon, S.W. and Kim, J.R. (2022), "Stability analyses of dual porosity soil slope", *Geomech. Eng.*, **28**(1), 77-87. https://doi.org/10.12989/gae.2021.28.1.077.

Skempton, A.W., Schuster, R.L. and Petley, D.J. (1969), "Joints and fissures in the London Clay at Wraysbury and Edgware", *Geotechnique*, **19**(2), 205-217. https://doi.org/10.1680/geot.1969.19.2.205.

Tran, A.T.P., Kim, A.R. and Cho, G.C. (2019), "Numerical modeling on the stability of slope with foundation during rainfall", *Geomech. Eng.*, **17**(1), 109-118. https://doi.org/10.12989/gae.2019.17.1.109.

Ukritchon, B., Yoang, S. and Keawsawasvong, S. (2020), "Undrained stability of unsupported rectangular excavations in non-homogeneous clays", *Comput. Geotech.*, **117**, 103281. https://doi.org/10.1016/j.compgeo.2019.103281.

Wang, L., Sun, D.A. and Li, L. (2019), "3D stability of partially saturated soil slopes after rapid drawdown by a new layer-wise summation method", *Landslides.*, **16**(2), 295-313. https://doi.org/10.1007/s10346-018-1081-2.

Weng, M.C., Lin, M.L., Lo, C.M., Li, H.H., Lin, C.H., Lu, J.H. and Tsai, S.J. (2019), "Evaluating failure mechanisms of dip slope using a multiscale investigation and discrete element modelling", *Eng. Geol.*, **263**, 105303. https://doi.org/10.1016/j.enggeo.2019.105303.

Yang, X.L. and Li, Z.W. (2018), "Comparison of factors of safety using a 3D failure mechanism with kinematic approach", *Int. J. Geomech.*, **18**(9), 04018107. https://doi.org/10.1061/(ASCE)GM.1943-5622.0001235.

Yang, X.L. and Xu, J.S. (2017), "Three-dimensional stability of two-stage slope in inhomogeneous soils", *Int. J. Geomech.*, **17**(7), 06016045. https://doi.org/10.1061/(ASCE)GM.1943-5622.0000867.

Zhang, F., Leshchinsky, D., Baker, R., Gao, Y.F. and Leshchinsky, B. (2016), "Implications of variationally derived 3D failure mechanism", *Int. J. Numer. Anal. Methods Geomech.*, **40**(18), 2514-2531. https://doi.org/ 10.1002/nag.2543.

Zhang, H.T., Luo, X.Q., Bi, J.F., He, G.F. and Guo, Z.J. (2019), "Submarine slope stability analysis during natural gas hydrate dissociation", *Mar. Geores. Geotechnol.*, **37**(4), 467-476. https://doi.org/10.1080/1064119X.2018.1452997.

Zhang, Y.B., Chen, G.Q., Zheng, L., Li, Y.G. and Zhuang, X.Y. (2013), "Effects of geometries on three-dimensional slope stability", *Can. Geotech. J.*, **50**(3), 233-249. https://doi.org/10.1139/cgj-2012-0279.

Zhou, J.F and Qin, C.B. (2020), "A novel procedure for 3D slope stability analysis: lower bound limit analysis coupled with block element method", *Bull. Eng. Geol. Environ*, **79**(4), 1815-1829. https://doi.org/10.1007/s10064-019-01657-1.

Zhou, Y., Zhang, F., and Li, B. (2019), "Static and seismic stability charts for three-dimensional cut slopes and natural slopes under short-term undrained conditions", *Adv. Civ. Eng.*, **2019**, 191467. https://doi.org/10.1155/2019/1914674.

GC

Notation

c_u	undrained shear strength
c_{u0}	initial undrained shear strength at the slope crest
γ	unit weight of soil
H	slope height
H'	height of the face failure mechanism
L	length of AB
B	width of the failure mechanism
β	slope angle
k	soil strength gradient in the depth direction
α	c_u profile inclination
M	dimensionless strength gradient parameter
r_0	radius of the lower boundary log-spiral
r_0'	radius of the upper boundary log-spiral
r_m	average radius of the two log-spirals
R	radius of the cross-sectional circle
θ_0	initial angle of the failure mechanism
θ_h	terminal angle of the failure mechanism
W_γ^{3D}	work rate done by soil weight of the torus
W_γ^{2D}	work rate done by soil weight of the plane insert
W_γ	total work rate done by soil weight
D^{3D}	internal energy dissipation rate of the torus
D^{2D}	internal energy dissipation rate of the plane insert
D_{int}	total internal energy dissipation rate
F_s	safety factor
N_s	stability number